International Journal of Biological Macromolecules 331 (2025) 148333

Contents lists available at ScienceDirect

International Journal of Biological Macromolecules

journal homepage: www.elsevier.com/locate/ijbiomac

Protein thermostabilization with *Protposer*: Pushing the stability limits and folding reversibility of a highly-stabilized apoflavodoxin

Antonio Hidalgo-Toledo [a,b], Darío Bazco [a,b], Víctor Correa-Pérez [a,b], Marta Martínez-Júlvez [a,b], Javier Sancho [a,b,c,*]

[a] *Biocomputation and Complex Systems Physics Institute (BIFI)-Joint Unit: GBsC-CSIC, University of Zaragoza, 50018 Zaragoza, Spain*
[b] *Departamento de Bioquímica y Biología Molecular y Celular, Faculty of Science, University of Zaragoza, 50009 Zaragoza, Spain*
[c] *Aragon Health Research Institute (IIS Aragón), 50009 Zaragoza, Spain*

ARTICLE INFO

Keywords:
Protein thermostabilization
Computational protein design
Protein stabilization
Apoflavodoxin
Stabilizing mutations
Protein stability

ABSTRACT

Enhancing the stability of highly stable proteins represents an interesting challenge in protein design. We have used the computational tool *Protposer* to rapidly achieve large additional stabilization of apoflavodoxin, a protein strongly thermostabilized over the years through protein engineering based on educated guesses. By rationally combining top-ranked mutations onto a previously stabilized variant (6 M), we have generated a series of new mutants and characterized their stability by thermal and chemical denaturation. Relative to the starting variant, the T_m of 10 M apoflavodoxin is nearly 9 °C higher, while the simplified 3 M and 4 M mutants, showing improved refolding properties, display increases of 6/7.5 °C, respectively. The thermostabilizing effects of individual mutations are close to additive and translate into a large increase in conformational stability at 25.0 °C. Comparison of the x-ray structures of progressively stabilized WT, 6 M and 10 M flavodoxins reveals a concomitant mild trend toward shorter hydrogen bonds, reduced internal cavity volumes and narrower tunnels. Overall, these conformational changes are minor, and a functional assay confirms the mutants also preserve their catalytic activity. These findings demonstrate that even highly stable proteins can be further stabilized through rational design using a simple computational tool that automatically analyses PDB files and identifies stabilizing mutations.

1. Introduction

The functional properties of most proteins are linked to the stability of their native conformation [1]. As the stability of proteins is characteristically low and tends to be further reduced ex vivo, the use of proteins as medicines [2,3], biocatalysts [4] or key components of all kind of analytical tests [5] is challenging [6]. One straightforward strategy to stabilize proteins is replacing specific amino acid residues by others that, given their structural context, make the protein more stable [7]. The difficulty is in identifying successful replacements. For that, many rational approaches based on physicochemical principles as well as on evolutionary considerations have been tried [8]. As the success rate obtained in the design of stabilizing mutations is not very high, computational tools have been devised to rationalize further the choice of stabilizing mutations [9–14]. In many cases the goal of those tools has been to predict the change in stability (ΔΔG) associated to a mutation. Unfortunately, the error bar of those predictions continues being high, as it is in the range of the expected stabilizing effect of mutations [15–19]. Trying to overcome this limitation, an alternative computational approach to stabilize proteins has been recently introduced that, rather than calculating ΔΔG values, classifies mutations as either significantly stabilizing or not, and provides the estimated success rate for each mutation proposed [20].

Over the years, our group has been using a variety of approaches to increase the conformational stability of the model protein apoflavodoxin [21]. They include, electrostatics [22,23], α-helix [24], H-bonding [25], packing [26] and solvent exposure optimization [27] as well as sequence consensus analysis [28]. By combining stabilizing mutations painfully discovered, wild type apoflavodoxin has been greatly stabilized and the cooperativity of its thermal folding equilibrium improved [28,29]. Feeling that we have exhausted our capabilities to intuitively designing stabilizing mutations for this protein, we explore here the use of *Protposer* [20] to further increase thermostability, as well as conformational stability at 25 °C. *Protposer* (https://protposer.bifi.es/) is a

* Corresponding author at: Biocomputation and Complex Systems Physics Institute (BIFI)-Joint Unit: GBsC-CSIC, University of Zaragoza, 50018 Zaragoza, Spain.
E-mail address: jsancho@unizar.es (J. Sancho).

https://doi.org/10.1016/j.ijbiomac.2025.148333
Received 17 July 2025; Received in revised form 1 October 2025; Accepted 14 October 2025
Available online 15 October 2025

computational tool designed to identify stabilizing mutations. To that end, it integrates a protein sequence and structure scanning engine with a logistic regression model that nominates and classifies mutations in an unsupervised manner. Given an input protein structure (PDB file or AlphaFold model), the algorithm systematically searches for structural or sequence features associated with instability, such as divergence from consensus or ancestral sequences, suboptimal α-helix composition, unfavorable residue solvent exposure, internal cavities, electrostatic imbalance, or destabilizing hydrogen bonds. For each identified "weak spot", *Protposer* proposes point mutations and evaluates their likelihood of enhancing stability. The evaluation brings together multiple structural and sequence-based criteria within a logistic regression model, which estimates the probability that a given mutation will increase conformational stability by at least 0.5 kcal/mol. The output is a ranked list of candidate stabilizing mutations, accompanied by a rationale for each proposal and a feature-based scoring breakdown, presented in an HTML summary. By merging established strategies for rational protein stabilization with machine learning, *Protposer* provides a practical and automated pipeline for guiding protein engineering efforts. A quick implementation of some of the top ranked mutations obtained with *Protposer* using only the PDB code as input has led to a substantial increase in apoflavodoxin stability in a short time.

2. Materials and methods

2.1. Design of mutants

New mutants of the apoflavodoxin from *Anabaena* PCC 7119 were designed using the *Protposer* software [20]. Apoflavodoxin mutations were selected from the ranked list of stabilizing proposals, excluding those labeled as affecting the active site. As the aim was to further stabilize a previously engineered and highly stable mutant referred to as 6 M [28,29], the six mutations already present in it were not considered either. Those mutations (I59A, I92A, D126K, A142V, E20K, and E72K) are also present in all new mutants that have been obtained and characterized in this work. From the *Protposer* list so cleaned, the best ranked 15 mutations were grouped to make three new mutants, each carrying five mutations: 5 M1 (D35K, I21K, D65K, D129K, L44F), 5 M2 (D43K, V76L D153K, N28G, D154E) and 5 M3 (V36L, Q48E, N79S, E61K, S158T). Mutant 5 M1 contains mutations ranked 1–3 and 5–6 (the five best ranked mutations with the exception of L44F (ranked 6) which replaces D43K, (ranked 4) to avoid pooling in 5 M1 five charge reversal mutations). Mutant 5 M2 contains mutations ranked 4 and 7–10 and mutant 5 M3 contains mutations ranked 11–15. A new mutant (10 M) was constructed by combining the mutations in 5 M2 and 5 M3. In addition, ten new single mutants were generated, each one containing only one of the mutations in either 5 M2 or 5 M3. Thermal analysis of the single mutants identified four mutations (V36L, D154E, D153K and N79S) as particularly stabilizing, which were combined to create two new mutants: 3 M (V36L, D154E, D153K) and 4 M (V36L, D154E, D153K, N79S). All plasmids encoding apoflavodoxin mutants were obtained from GeneScript.

2.2. Overexpression and purification

Flavodoxin mutants were purified as previously described [30], with some modifications. To obtain a given flavodoxin variant, *E. coli* (BL21 strain), cells carrying the pTr99a plasmid containing the corresponding mutant gene were grown overnight in 50 mL of LB medium supplemented with ampicillin (100 μg/mL). 1 L of LB medium was inoculated with the culture and grown at 37 °C. When the optical density at 600 nm reached 0.6–0.8, 1 mL of 1 M isopropyl-β-D-thiogalactopyranoside was added and the culture continued overnight. Cells were harvested using a high-speed centrifuge (2236R High Speed Centrifuge, Gyrozen) with a rotor with capacity for 6 1-L bottles (GRF-L-1000-6, Gyrozen), at 6000 rpm during 15 min, and the cell paste was collected and stored at −80 °C. After thawing, the cell paste was resuspended in the least quantity needed of 50 mM Tris-HCl, pH 8.0 for total resuspension. A small amount (2 mg) of flavin mononucleotide (FMN) (Sigma-Aldrich) was added to the suspension and completely dissolved. The suspension was placed in an ice bath and sonicated (UP 200S, Hielscher Ultrasonics GmbH) with 8 cycles of 45 s at 70 % amplitude, with 30 s rest intervals between cycles. The sonicated suspension was centrifuged at 18000 rpm for 30 min in a 50 mL bottle rotor (GRF-L-50-6, Gyrozen) and ammonium sulfate (Panreac Applichem) was added to the supernatant to reach 60 % saturation at 0 °C. The suspension was centrifuged at 20000 rpm for 30 min to remove unwanted proteins, and the supernatant was loaded into an equilibrated HiTrap Capto DEAE 5 mL column (Cytiva) using a ÄKTA start system (Cytiva). The column was washed with 10 volumes of 50 mM Tris-HCl, pH 8.0, 60 % ammonium sulfate to remove unbound FMN and non-retained proteins. Then, flavodoxin was eluted using a gradient from 60 % to 0 % ammonium sulfate in the same Tris buffer. Fractions containing flavodoxin, as indicated by the UV/Vis spectrum, were dialyzed against 50 mM Tris-HCl pH 8.0 and then loaded into a HiTrap Capto DEAE 5 mL column (Cytiva) equilibrated in the same buffer. The column was washed with 10 volumes of equilibration buffer and the protein was eluted with a NaCl gradient (from 0 to 1 M). Fractions with a 464/280 absorbance ratio > 0.12 were dialyzed against 50 mM Tris-HCl, pH 8.0, pooled and stored. For mutants 5 M1 and 10 M the purification process was performed in a different way due to their weak binding to the DEAE matrix, probably caused by their low net charge at the purification pH. After performing the purification process, the fractions of these two mutants with a 464/280 absorbance ratio of approximately 0.12, were concentrated using centrifugal filters (Amicon Ultra-15 10 k, Sigma-Aldrich) and loaded into a Superdex 75 Increase 10/300 GL column (Cytiva) equilibrated in 50 mM Tris-HCl, pH 8.0 to perform a gel filtration using a ÄKTA Go system (Cytiva). The elution buffer for the gel filtration was the same in which the column was equilibrated. Fractions with a 464/280 absorbance ratio > 0.12 were pooled and stored frozen until use.

2.3. Preparation of apoflavodoxin

For most mutants, FMN was removed from the holoprotein using a treatment with trichloroacetic acid, as described [31]. Dithiothreitol (DTT) (Sigma-Aldrich) up to 1 mM and trichloroacetic acid (TCA) (Thermo Fisher Scientific) up to 3 % (*w/v*) at 0 °C were added to the holoflavodoxin solution, causing the protein to precipitate. The protein was centrifuged at 5000 rpm for 5 min and the pellet resuspended and washed in 1 mL of 1 mM DTT/3 % TCA, and the protein was pelleted again. This washing step was repeated until the pellet became white. The final pellet was resuspended in 1 M MOPS, pH 7.0 (Thermo Fisher Scientific) and dialyzed against 50 mM MOPS, pH 7.0. Purity of all apoflavodoxin solutions so prepared were > 98 % as judged from SDS-PAGE (Fig. S1). For mutants 5 M1 and 10 M, apoflavodoxin was obtained using an alternative method including unfolding and refolding steps. A solution of holoflavodoxin was added to a solution of 6 M guanidinium chloride in 50 mM MOPS, pH 7.0 to a final guanidinium concentration of 5 M and it was incubated at 37 °C for 1 h in the dark. The FMN released was separated from the solution using centrifugal filters (Amicon Ultra-15 10 k, Sigma-Aldrich) and then the buffer of the protein solution was changed to 50 mM MOPS, pH 7.0, using the same filters. Purity of these apoflavodoxin preparation was >95 % as judged from PAGE.

2.4. Circular dichroism and fluorescence spectra

Circular dichroism (CD) spectra were registered at 15 °C in a Chirascan apparatus (Applied Photophysics). For both near-UV CD and far-UV CD, 20 μM protein samples dissolved in 50 mM MOPS, pH 7.0 buffer were used. Near-UV spectra were recorded from 310 to 260 nm in a 4-mm path-length cuvette. Far-UV CD spectra were recorded from 260 to 190 nm in a 1-mm path-length cuvette. Fluorescence spectra (from

360 to 320 nm, with excitation at 280 nm) of 2 μM protein samples were obtained using a Cary Eclipse fluorimeter (Agilent Technologies).

2.5. Thermal denaturation curves

Thermal denaturation curves were obtained using the same protein concentration, buffer and cuvette path-length and equipment as described above for the CD and fluorescence spectra. The denaturation curves were followed measuring the signal at 222 nm in far-UV CD, 290 nm in near-UV CD, and the 360/320 ratio of fluorescence intensities, with excitation at 280 nm. As reported previously [32], recording fluorescence intensity ratios is useful to minimize the strong temperature dependence of the folded and unfolded baselines but it may slightly modify the value of the observed T_m. However, it hardly modifies the value of differences between ΔT_m between variants of the same protein [33]. In all experiments the temperature was raised from 290.15 to 365.15 K at a rate of 1 K/min.

2.6. Differential scanning calorimetry (DSC)

The protein samples for differential scanning calorimetry were prepared at a 20 μM protein concentration in 50 mM MOPS, pH 7.0. The experiments were performed in a MicroCal Differential Scanning Calorimeter (Malvern Instruments) from 10 °C to 95 °C at a scan rate of 1 °C/min. For all measurements 50 mM MOPS, pH 7.0 buffer was used in the reference cell of the calorimeter. The baseline was recorded after filling both calorimeter cells with buffer prior to performing the experiments, and several buffer–buffer baselines were recorded prior to each run with a protein sample to ensure a proper equilibration of the instrument [23].

2.7. Analysis of thermal unfolding data

The data from thermal denaturation curves followed by near-UV CD, far-UV CD and fluorescence were roughly normalized between 0 and 1 and globally fitted to either 2-state or 3-state models using Origin 9.0 (OriginLab Corporation). Eq. 1 was used to fit the curves to the two-state model, and Eq. 2 to fit to the three-state one [23].

$$Y = \frac{Y_N + m_N T + (Y_D + m_D T)e^{-\Delta G/RT}}{1 + e^{-\Delta G/RT}} \quad (1)$$

$$Y = \frac{Y_N + m_N T + (Y_i + m_i T)e^{-\Delta G_1/RT} + (Y_D + m_D T)e^{-(\Delta G_1 + \Delta G_2)/RT}}{1 + e^{-\Delta G_1/RT} + e^{-(\Delta G_1 + \Delta G_2)/RT}} \quad (2)$$

In these equations [23,32], Y corresponds to the signal registered by the dichrograph or fluorimeter, T is the absolute temperature, Y_N, Y_i and Y_D are, respectively, the signals of the protein in the native, intermediate and denatured states at $T = 0$, m_N, m_i and m_D are the slopes of the temperature dependency of the native, intermediate and denatured states signals and ΔG is given by the Gibbs–Helmholtz equation (Eq. 3)

$$\Delta G = \Delta H(1 - T/T_m - \Delta Cp)(T_m - T + Tln(T/T_m)) \quad (3)$$

From a global fitting of the near-UV CD, far-UV CD and fluorescence curves corresponding to a protein variant, the thermodynamic parameters describing the unfolding equilibrium are obtained (ΔH, T_m and ΔC_p for a 2-state fit, and ΔH_1, T_{m1}, ΔCp_1, ΔH_2, T_{m2} and ΔC_{p2} for a 3-state fit), together with several spectroscopic parameters, which are specific of each curve and have no thermodynamic meaning or influence on the value of the common thermodynamic parameters shared by the curves (e.g the melting temperatures do not change if molar ellipticity is used instead of mdeg for circular dichroism). Unlike ΔH and T_m values, the values obtained for ΔC_p in these global fits are not accurate [34], so they will not be reported. The DSC unfolding data was normalized to concentration and analyzed using a two-state or three-state model, as implemented in the Origin 7.0 package.

2.8. Thermal denaturation reversibility

The thermal denaturation reversibility was studied by DSC, near-UV CD and fluorescence with protein dissolved in 50 mM MOPS, pH 7.0. For DSC and near-UV CD, the samples were prepared at a 20 μM protein concentration and, for fluorescence, at 2 μM. DSC experiments were performed recording from 10 °C to 90 °C, allowing the sample to cool down, and then recording the denaturation again up to 90 °C at a scan rate of 1 °C/min. For fluorescence and near-UV CD, a denaturation curve from 15 °C to 90 °C was recorded, followed by rapidly cooling the sample to 15 °C and then recording a new denaturation curve. The percentage of reversibility was obtained comparing the ΔH_{cal} obtained in the first DSC scan or denaturation curve measured by fluorescence or near-UV CD with the second one performed after cooling.

2.9. Urea denaturation curves and data analysis

The protein solutions were made as described [28] with minor variations. 100 μL of 20 μM apoprotein in 50 mM MOPS, pH 7.0 were mixed with 900 μL of urea solutions (from 0 to 7 M) in 50 mM MOPS, pH 7.0. The samples were equilibrated at 25 °C for 30 min and the denaturation was followed at 25 °C recording fluorescence at 320 nm with excitation at 280 nm, using a thermostated Cary eclipse fluorimeter (Agilent Technologies). As flavodoxin unfolding in urea follows a 2-state mechanism [30], the curves were fitted to Eq. 4, using Origin 9.0 (OriginLab Corporation) assuming that the free energy of denaturation varies linearly with urea concentration (Eq. 5), as described [26].

$$S = \frac{S_F + m_F D + (S_U + m_U D)e^{(-\Delta G/RT)}}{1 + e^{(-\Delta G/RT)}} \quad (4)$$

$$\Delta G = \Delta G_w - mD = m(U_m - D) \quad (5)$$

In Eq. 4, S corresponds to the signal registered by the fluorimeter, T is the absolute temperature, S_F, and S_U are, respectively, the signals of the protein in the folded and unfolded state, m_F and m_U are the slopes of the urea dependency of the folded and unfolded state signals, R is the ideal gas constant, ΔG is the free energy of unfolding. In Eq. 5, m is a proportionality constant and U_m is the urea concentration of mid-denaturation. [26].

2.10. Cytochrome c reductase activity

All stock samples for this experiment were dissolved in 50 mM Tris-HCl, pH 8.0. Measurements were made at 25 °C in a Cary 3500 Multicell UV–Vis spectrophotometer (Agilent Technologies). Stock solutions of the reagents used for this reaction (Scheme 1) were 7.5 mg/mL cytochrome *c* (Thermo Fisher Scientific), 1 mM NADPH (Sigma-Aldrich), 0.1–0.8 mM flavodoxin, and 2.5–5.0 μM FNR. The volumes of stock solutions used in a typical assay, together with the electron transfer reaction measured, are those in scheme 1. After adding all the other reagents to the sample cuvette, FNR was deposited on the upper end of the inner wall of the cuvette and the reaction started by inverting the cuvette three times. The kinetic reaction was measured for 30 s at a wavelength of 550 nm. Kinetics were recorded at different flavodoxin concentrations and the corresponding initial velocities were fitted to the Michaelis-Menten equation (Eq. 6).

$$V = \frac{v_{max}[S]}{K_m + [S]} \quad (6)$$

2.11. Protein crystallization and structure resolution of mutant 10 M in complex with FMN

Crystals of holoflavodoxin mutant 10 M were obtained using the hanging-drop vapor-diffusion method at 291 K. Each drop consisted of 1 μL of 5 mg/mL holoflavodoxin in 10 mM Tris-HCl, pH 8.5, plus 1 μL of

Scheme 1: Protocol for preparing cytochrome c reductase activity solutions, and the electron transfer flow in the reaction

Reagent	Sample (µL)	Reference (µL)
Tris-HCl (50 mM)	850 – x	900
cytochrome c (7.5 mg/mL)	100	100
NADPH (1 mM)	50	-
Flavodoxin (0.1-0.8 mM)	x	-
FNR (2.5-5.0 µM)	2	-

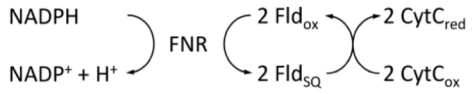

Scheme 1. Protocol for preparing cytochrome *c* reductase activity solutions, and the electron transfer flow in the reaction

reservoir solution. The drops were equilibrated against 500 µL of reservoir solution. Crystals suitable for X-ray diffraction were obtained in the condition 28 % PEG 4000, 0.1 M Tris-HCl, pH 8.5 and 0.2 M $MgCl_2$. The crystals reached their maximum size in one week and were cryoprotected with 20 % of glycerol before diffraction data collection. Data were collected from a single crystal using the synchrotron source DLS beamline BL13-XALOC and PILATUS3 X 6 M (100 Hz) detector with a wavelength of 0.979260 Å, to a maximum resolution of 1.4 Å. Crystals belonged to the $P2_12_12_1$ orthorhombic space group with two molecules in the asymmetric unit. Data set was processed, scaled and reduced using XDS [35] and SCALA from CCP4i package [36,37]. The structure was solved by molecular replacement using the MOLREP program from CCP4i [38] with the structure of wild-type holoflavodoxin (PDB ID: 1FLV) as the search model. Automatic refinement was performed by Refmac5 [39] from the CCP4i package, combined with alternating manual model building in WinCOOT [40]. The final model includes residues 2–169, one FMN molecule, one glycerol molecule and 236 water molecules. Relevant data collection statistics and refinement parameters are presented in Table S1. The coordinates and structure factors for apoflavodoxin mutant 10 M in complex with FMN have been deposited in the Protein Data Bank with PDB ID: 9RXF. The program PyMOL was used for the superposition with RMSD calculation and visualization of the structures [41], and Biopython for identification of hydrogen bonds [42].

3. Results

3.1. Mutant purification and apoflavodoxin preparation

Protein purification and apoflavodoxin preparation was done as reported [30,31] except for mutants 5 M1 and 10 M. Possibly because of their reduced net charge at the pH used for the purification, their binding to the DEAE column was less tight and their purification required an additional gel filtration step, as described in Methods. Once the holoforms of these two mutants were obtained, the preparation of the corresponding apoflavodoxins by precipitation with TCA was not possible as their precipitates did not refold properly. Thus, their apo forms were obtained using a different procedure as described in Methods. The 5 M1 and 10 M apoflavodoxins so obtained displayed the typical near UV CD apoflavodoxin spectrum [30], as shown in Fig. 1.

3.2. Mutants thermostability as determined by CD and fluorescence

Thermal denaturation curves were recorded for each mutant by monitoring tryptophan emission fluorescence, near-UV CD and far-UV CD. For each mutant, a global analysis of the three curves was performed to determine the melting temperature and the apparent

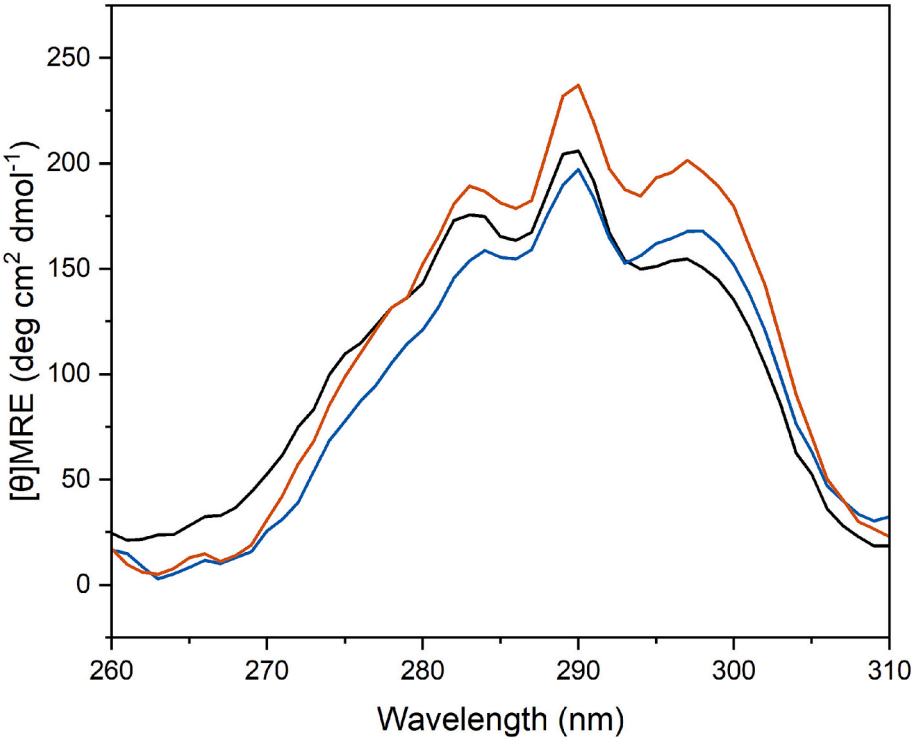

Fig. 1. Near UV CD spectra of the apo form of two apoflavodoxin mutants (5 M1, orange; and 10 M, black line) obtained by unfolding/refolding (see Methods), compared to the spectrum of 6 M (blue line), obtained by TCA precipitation. Protein concentration was 20 µM in all cases.

unfolding enthalpy following a previously described approach [43]. It is well established that wild type apoflavodoxin experiences a three-state thermal unfolding [44], while some carefully stabilized mutants (e.g., 6 M) are two-state [29]. The data recorded for the new mutants have been fitted to both two-state and three-state thermal unfolding models to determine their equilibrium unfolding mechanisms. The previously reported 6 M mutant [28,29], which act in this study as a starting pseudo wild type, has been re-examined, as it constitutes the reference protein to judge the thermostabilization afforded by the new mutations here introduced. In agreement with the initial report [28], the unfolding mechanism of 6 M is well described by a two-state model (Fig. 2a, Table 1) with a single T_m of 70.1 ± 0.3 °C, which compares well with the values of 70.3 ± 0.1 °C (reported previously [28] by DSC) and also with the value of 70.4 ± 0.2 °C obtained in new DSC experiments done for this work (see Table 2).

Of the three new apoflavodoxin mutants (5 M1, 5 M2 and 5 M3) where five mutations have been added to 6 M, mutant 5 M1 failed to stabilize it. In fact, mutant 5 M1 reverted from the two-state behavior displayed by 6 M to the three-state behavior characteristic of the original wild type protein [44], and its higher T_m (T_{m2}) was 69.0 ± 1.2 °C (not shown). While in revision, we have been able to trace this unwanted effect to mutation D129K (see Fig. S2). In contrast, mutants 5 M2 and 5 M3 retain the two-state equilibrium unfolding of 6 M and display higher T_m values of 74.5 ± 0.3 °C and 72.7 ± 0.8 °C, respectively. Thus, the thermostability of 5 M2 and 5 M3 has been increased by 4.4 and 2.6 °C, compared to 6 M. As the effect of protein stabilizing mutations tends to be additive [29], we then combined the mutations in 5 M2 and 5 M3 to produce the 10 M mutant. An initial global analysis of its unfolding curves (not shown) raised doubts on whether it retained the two-state behavior of 6 M. As indicated above, and similarly to 5 M1, the 10 M mutant showed a low tolerance to the acidic pH used to prepare the apo form, which complicated its purification (Fig. S3). In addition, 10 M also shows a low tolerance to freezing: a high percentage of the protein precipitates upon thawing and, according to near-UV CD (Fig. S4), the soluble part displays an altered structure. Thus, to clarify the unfolding mechanism of 10 M, we performed new spectroscopic measurements in a sample that had not been previously frozen. This analysis confirmed that 10 M retains a two-state unfolding mechanism, with a T_m of 79.3 °C, 9.2 °C higher than that of 6 M (Table 1, Fig. 2b).To identify the specific mutations responsible of the high thermostability of 10 M and to be able to discard those that yield the observed poor behavior at the low pH needed for the preparation of its apo form, 10 new mutants were produced and tested. These mutants were based on 6 M, with the mutations from 10 M incorporated individually. After analysis of these mutants, the most stabilizing mutations: V36L (ΔT_m = 3.8 °C), D153K (ΔT_m = 2.5 °C), D154E (ΔT_m = 1.1 °C) and N79S (ΔT_m = 1.0 °C) were grouped in two final mutants, termed 3 M and 4 M, both of which present a fine pH stability and do not aggregate after the TCA precipitation step used

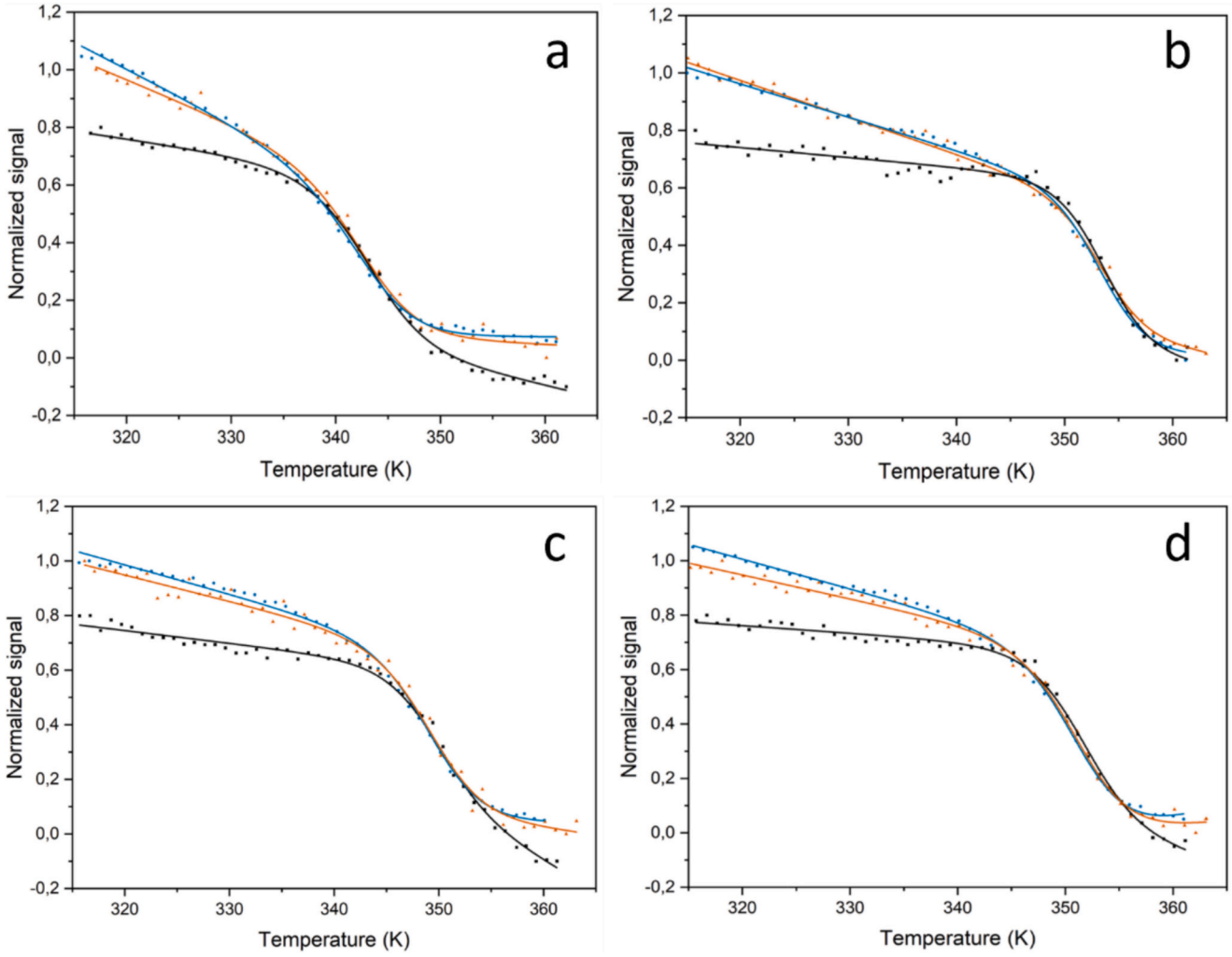

Fig. 2. Thermal denaturation curves (far-UV CD: black squares, near-UV CD: blue dots, and fluorescence: orange triangles) of 6 M and the most stabilizing new variants: 10 M, 3 M and 4 M, are shown. (a) 6 M; (b) 10 M; (c) 3 M; (d) 4 M. The global fitting to a two-state equation of the three curves corresponding to each variant are shown as solid lines.

Table 1
T_m and ΔH values for apoflavodoxin mutants as determined from global fitting of spectroscopically monitored thermal unfolding curves to a two-state model.

Variant	T_m (°C)	ΔH (kcal/mol)
6 M[b]	70.1 ± 0,3	72.7 ± 8.3
5 M1[a]	–	–
5 M2	74.5 ± 0,3	91.2 ± 3.0
5 M3[b]	72.7 ± 0,8	82.9 ± 1.9
10 M[c]	79.3 ± 1,0	109.2 ± 3.2
D153K[b]	72.6 ± 0,0	78.6 ± 7.6
D154E[b]	71.2 ± 0,7	75.6 ± 1.0
N28G[b]	70.6 ± 0,4	79.0 ± 9.0
V76L[b]	67.6 ± 0,9	56.9 ± 9.3
D43K[b]	70.8 ± 0,0	78.3 ± 4.2
Q48E[b]	69.2 ± 0,8	73.5 ± 1.0
V36L[b]	73.9 ± 0,1	83.3 ± 0.6
E61K[b]	70.8 ± 0,0	88.0 ± 9.0
N79S[b]	71.1 ± 0,1	67.5 ± 3.8
S158T[b]	68.4 ± 0,4	84.6 ± 6.4
3 M[b]	76.2 ± 0,1	77.8 ± 1.1
4 M[b]	77.9 ± 0,0	97.4 ± 3.0

[a] The thermal unfolding equilibrium of this variant is three-state. The fitted values of the two transition temperatures and unfolding enthalpies are, in °C and kcal/mol, respectively: T_{m1}=59.7±0.9; ΔH_1=121±2; T_{m2}=69.1±1.2 and ΔH_2=109±3.
[b] The reported values of T_m and ΔH are means of two determinations ± SE.
[c] The reported value of T_m and ΔH is a mean of three determinations ± SE.

Table 2
T_m and ΔH values for apoflavodoxin mutants as determined from DCS.

Protein	T_m(°C)	ΔH_{cal} (kcal/mol)	ΔH_{vH}	$\frac{\Delta H_{vH}}{\Delta H_{cal}}$
6 M[a]	70.4 ± 0.2	83.2 ± 2.5	91.8 ± 4.2	1.10
5 M1[b]	67.9 ± 0.1	60.5 ± 1.3	137.5 ± 6.2	2.27
5 M2[b]	74.4 ± 0.1	89.0 ± 3.7	95.9 ± 10.4	1.08
5 M3	73.0 ± 0.1	80.1 ± 0.2	88.3 ± 0.3	1.10
10 M[b]	79.0 ± 0.4	97.7 ± 1.7	113.1 ± 4.5	1.16
D153K	71.8 ± 0.1	95.0 ± 0.2	94.5 ± 0.2	0.99
D154E	71.7 ± 0.1	89.0 ± 0.2	92.6 ± 0.2	1.04
N28G	71.6 ± 0.1	85.6 ± 0.5	88.9 ± 0.6	1.04
V76L	70.1 ± 0.1	74.8 ± 0.2	72.2 ± 0.2	0.97
D43K	69.3 ± 0.1	74.7 ± 0.1	80.6 ± 0.2	1.08
Q48E	70.0 ± 0.1	87.2 ± 0.1	89.7 ± 0.1	1.03
V36L	73.5 ± 0.1	87.9 ± 0.1	90.0 ± 0.1	1.02
E61K	71.5 ± 0.1	88.6 ± 0.1	102.1 ± 0.2	1.15
N79S	71.8 ± 0.1	86.5 ± 0.2	97.0 ± 0.2	1.12
S158T	70.2 ± 0.1	88.6 ± 0.3	80.4 ± 0.3	0.91
3 M[b]	76.5 ± 0.4	105.4 ± 0.3	107.9 ± 1.8	1.02
4 M	77.7 ± 0.1	108.5 ± 2.0	112.5 ± 0.4	1.04

[a] The reported value of T_m and ΔH is a mean of three determinations ± SE.
[b] The reported values of T_m and ΔH are means of two determinations ± SE.

for apoprotein preparation. The 3 M T_m of 76.2 °C is 6.1 °C higher than that of 6 M (Table 1, Fig. 2 c), and the 4 M T_m of 77.9 °C is 7.8 °C higher (Table 1, Fig. 2 d).

3.3. Mutants thermostability as determined by DSC

The thermostability of all the mutants as well as their thermal unfolding mechanism have also been determined by DSC (Fig. 3). Analysis of the thermograms indicates that both 5 M2 and 5 M3 comply to a two-state equilibrium thermal unfolding, as judged from their $\Delta H_{VH}/\Delta H_{cal}$ ratios of 1.08 and 1.10.

Relative to 6 M, the 5 M2 and 5 M3 T_ms are 4.0 and 2.6 °C higher (Table 2, Fig. 3), respectively, which is in good agreement with the thermostabilizations of 4.4 and 2.6 °C derived from the analysis of the thermal unfolding curves (Table 1). The 10 M mutant showed an increase in T_m of 8.6 °C and according to its $\Delta H_{VH}/\Delta H_{cal}$ ratio of 1.16 it seems it follows a two-state equilibrium (Table 2). The ten mutants built on 6 M individually incorporating the mutations in 10 M appear to

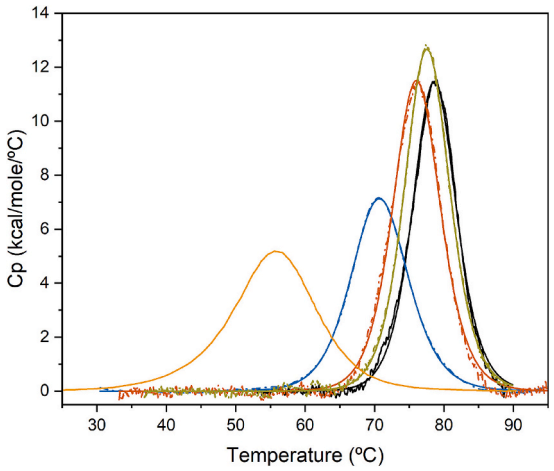

Fig. 3. DSC thermograms of the most stable variants (10 M: black, 3 M: orange, 4 M: olive) compared to 6 M (blue) and WT apoflavodoxin (yellow). The experimental data are represented as dash-dots and the fits to either a two-state model (6 M, 10 M, 3 M and 4 M) or a three-state model (WT) as solid lines. The thermogram of the WT protein was taken from [28].

follow a two-state mechanism, according to the $\Delta H_{VH}/\Delta H_{cal}$ ratios from 0.91 to 1.15 (Table 2). The more stabilizing ones are: V36L, D153K, D154E and N79S, which increased the T_m by 3.1, 1.4, 1.3 and 1.4 °C, respectively. The 3 M mutant (V36L, D153K and D154E) has a T_m 6.1 °C higher than that of 6 M (Table 2), which coincides with the thermostabilization of 6.1 °C determined from the spectroscopic analysis (Table 1). Its $\Delta H_{VH}/\Delta H_{cal}$ ratio of 1.01 confirms its thermal unfolding is two-state. The 4 M mutant (3 M plus N79S) has a T_m 7.3 °C higher than 6 M (Table 2), which is consistent with the stabilization of 7.8 °C observed by spectroscopy (Table 1). Fig. 3 shows the thermograms of 6 M, 10 M, 3 M and 4 M, compared to that of WT apoflavodoxin.

3.4. Thermal denaturation reversibility

The reversibility of the thermal unfolding of WT apoflavodoxin has been reported to be as high as 90 % when the heating is stopped at 65 °C, close to the end of the second unfolding transition of its three-state unfolding process [25,44]. Reversibility, however, is lower if the heating reaches higher temperatures. Because the apoflavodoxin variants here examined unfold at quite higher temperatures, reversibility studies have been conducted on 6 M, 10 M, 3 M and 4 M, to determine whether their thermal unfolding is reversible and, in such case, the percentage of unfolded protein that is able to refold after denaturation at 90 °C. For that, consecutive DSC thermal denaturations from 10 to 90 °C have been conducted on each variant, with cooling in between. For each variant,

Table 3
Thermal unfolding reversibility of 6 M, 10 M, 3 M and 4 M.

Near-UV CD and fluorescence					
Mutant	T_m[a] (°C)	T_m[b] (°C)	ΔH_{unf}[a] (Kcal/mol)	ΔH_{unf}[b] (Kcal/mol)	reversibility[c] (%)
6 M	68.9 ± 0.3	68.5 ± 0.3	76.1	61.5	81
10 M	81.1 ± 1.2	79.7 ± 0.2	85.9	81.3	95
3 M	75.2 ± 0.5	75.8 ± 0.8	80.9	80.4	99
4 M	77.7 ± 0.2	78.3 ± 0.8	95.1	94.8	99
DSC					
6 M	70.2 ± 0.1	70.1 ± 0.1	84.6	35.4	42
10 M	78.7 ± 0.1	78.8 ± 0.1	95.9	57.2	60
3 M	77.0 ± 0.1	76.8 ± 0.1	105.6	72.4	69
4 M	77.8 ± 0.1	77.6 ± 0.1	106.5	93.1	87

[a] Before unfolding.
[b] After refolding.
[c] ΔH_{unf} (first)/ΔH_{unf} (second).

the calculated T_ms obtained were virtually identical (Table 3), indicating that the refolded protein is as stable as fresh one. Comparison of recovered ΔH values in consecutive unfoldings suggests the reversibility of refolding from 90 °C is of 42 % (6 M), 60 % (10 M), 69 % (3 M) and 87 % (4 M). Thus, the reversibility of 4 M unfolding doubles that of 6 M. It is noticeable that, compared with the similarly thermostable 3 M and 4 M mutants, 10 M present a lower reversibility, which adds to its poorer tolerance to acidic pH and its tendency to aggregate and precipitate after thawing. In addition to using DSC, reversibility has been also assessed from analogous consecutive thermal unfolding experiments followed by near-UV CD and fluorescence (Table 3). In these experiments the T_ms of the second scans are also the same as those of initial ones, and the observed reversibilities are higher (81, 95, 99 and 99 % for 6 M, 10 M, 3 M and 4 M, respectively). The quality of the refolded protein has also been assessed from comparison of the near-UV CD spectra before unfolding and after refolding. Although intensities may be different due to incomplete reversibility in some cases, the distinct shape of the spectrum is recovered (Fig. S5).

3.5. Mutants thermostability at 25 °C as determined by chemical denaturation

Chemical unfolding curves of the original WT protein, the 6 M pseudoWT reference variant and the two thermostabilized 3 M and 4 M variants were recorded following the fluorescence emission at 320 nm with excitation at 280 nm. As the chemical unfolding of WT and 6 M apoflavodoxin is two-state [28,30] the curves (Fig. 4) were fitted to a two-state equation (Eq. 4). The stability so determined at 25.0 °C for WT and 6 M (Table 4) agrees with previously reported data [28] and indicates that the 6 M reference mutant on which new mutations have been introduced in this work is about 2.8 kcal/mol more stable than the original WT. Compared to 6 M, the new 3 M and 4 M mutants here obtained are around 2.5 kcal/mol more stable at 25.0 °C, which indicates that their higher thermostability translates into a higher conformational stability at much lower temperatures.

Translation of ΔT_m into ΔΔG is the expected behavior for a variant exhibiting a higher T_m and ΔH and a similar ΔC_p. Although accurate ΔC_p values cannot be derived from the global fit of spectroscopically followed unfolding curves—and it is not without difficulty for very stable variants—, an approximation can be derived from linear plots of ΔH versus T_m for a family of variants with different thermostability.

Using this approach and the data in Tables 1 and 2, we calculated (Fig. 5), that the ΔC_p of apoflavodoxin variants exhibiting a two-state thermal unfolding equilibrium is 2.5–2.8 kcal/mol.K, which compares

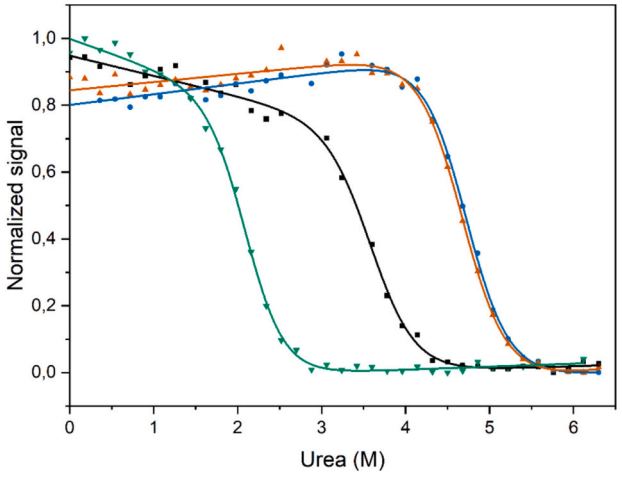

Fig. 4. Urea denaturation curves of WT (green triangles), 6 M (pseudoWT, black squares) and the stabilized 3 M (orange triangles) and 4 M (blue dots) apoflavodoxin mutants. Two-state fits are shown as solid lines.

Table 4
Chemical denaturation of apoflavodoxin variants. Conformational stability at 25 °C.

Mutant	m (kcal/mol M^{-1})	$[urea]_m$ (M)	ΔGw (kcal/mol)
WT	2.57 ± 0.17	2.11 ± 0.02	5.42 ± 0.36
WT[a]	2.48 ± 0.05	2.07 ± 0.01	5.13 ± 0.02
6 M	2.23 ± 0.21	3.61 ± 0.03	8.04 ± 0.77
6 M[a]	2.14 ± 0.08	3.78 ± 0.01	8.06 ± 0.01
3 M	2.26 ± 0.18	4.68 ± 0.04	10.55 ± 0.87
4 M	2.24 ± 0.16	4.71 ± 0.03	10.57 ± 0.77

[a] Data from Lamazares et al., 2015. Reported values of m, $[urea]_m$ and ΔG_w are means of two determinations ± SE.

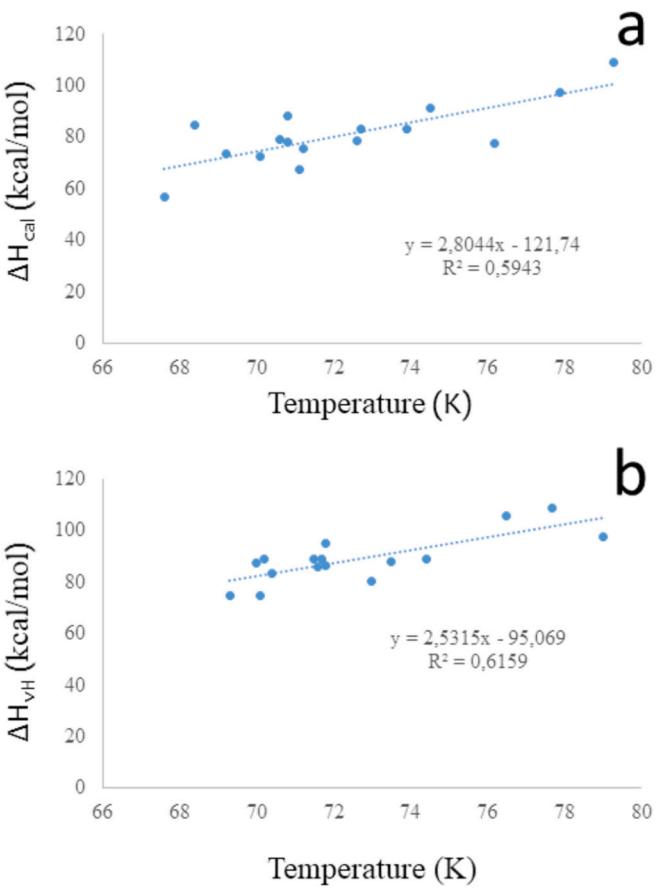

Fig. 5. Calculation of the folding heat capacity change in two-state apoflavodoxin variants from ΔH vs T plots. (a) vant Hoff ΔH values from global fits of spectroscopic curves (Table 1). (b) calorimetric ΔH values from DSC (Table 3).

well with the previously reported global ΔC_p change ($\Delta C_{p1} + \Delta C_{p2}$) of 2.5(±0.3) to 3.1(±0.8) kcal/mol.K [44] for the wild type protein. Since WT, 6 M, 10 M, 3 M and 4 M, all seem to have a common ΔC_p value and their unfolding enthalpies increase as they become more stable (as it is expected) the observed thermostabilizations (i.e., higher T_m values) translate into higher conformational stabilities at lower temperatures, as determined in the chemical denaturation experiments (Fig. 4).

3.6. Redox activity of the more stable mutants

Redox activity assays were conducted for 6 M and the stabilized 10 M, 3 M, and 4 M mutants to determine the Michaelis-Menten (K_M) and catalytic constant (k_{cat}) of the FNR enzyme in an electron transfer reaction (Scheme 1), where flavodoxin acts as the electron acceptor. The

reported K_M values (Table 5) refer specifically to the flavodoxin substrate. A comparison of the values with those previously reported for the WT flavodoxin [45], reveals that all flavodoxin variants remain catalytically active with the FNR enzyme, albeit with slightly reduced efficiencies. (Table 5). Previous analysis of the catalytic efficiency of flavodoxin variants that were not designed to increase the conformational stability revealed they were on average less catalytically efficient than the WT [46]. Comparison of the catalytic efficiencies of 12 such variants (Table 2 in [46] with those of the 4 variants in Table 5 (this work) indicates the two sets are not significantly different ($p = 0.22$ for Welch's *t*-test and $p = 0.50$ for non-parametric Mann–Whitney *U* test). Thus, the reduced efficiencies associated with the stabilizing mutations analyzed in this study are unlikely to result from their enhanced stability. Rather, they may arise from the extensive and mutation-sensitive nature of the flavodoxin/FNR binding interface [47,48], which is not annotated in the flavodoxin PDB file.

3.7. Crystal structure of 10 M. comparison with WT and 6 M

The crystal structure of the highly stabilized 10 M variant has been solved in its holo form. Comparison with the corresponding structures of the WT and 6 M holoflavodoxins previously reported [29,49] offers an opportunity to evaluate the impact of strong protein stabilization on the tridimensional structure. Overall, these three flavodoxins exhibit a very similar folding pattern, with their superposition yielding low r.m.s.d. values (10 M/WT: 0.263 Å for 146 Cα; 10 M/6 M: 0.185 Å for 139 Cα,) (Fig. 6). Most of the structural differences are concentrated in specific loop regions. In 10 M, loops 27–30 (bearing the N28G mutation) and 36–40 deviate from their positioning in WT and 6 M, and the 133–137 loop adopts a different folding arrangement in each structure.

The three structures have been compared in search for differences in hydrogen bonding. Our analysis indicates that the lengths of homologous hydrogen bonds are significantly shorter in either of the more stable variants (6 M and 10 M) than in WT (Fig. 7). Specific comparison of 6 M and 10 M also suggests that hydrogen bonds are shorter in the more stable 10 M variant than in 6 M but, in this case, the difference is not statistically significant.

The ten hydrogen bonds exhibiting the greatest shortening are shown in Fig. S6. Among these, the most significantly shortened one are R112:V76—reduced from 3.19 Å in the WT to 2.84 Å in 6 M, and 2.91/2.48 Å in 10 M (chains A/B); R112:V76—and G27:R23—from 3.44 Å (WT) to 3.05 Å (6 M) and 3.13/3.12 Å (10 M, chains A/B). Seven of these shortened bonds involve backbone nitrogen and oxygen atoms. Notably, four of them, along with three additional bonds involving also side chain atoms, contain polar residues located on the protein surface (i.e., R112:V76, G27:R23, G168:S65, S17:G13, R155:Q148, S37:D35, and R134:K137). This pattern suggests that the surface shell of the stabilized mutants may be slightly more compact compared to the WT. Of interest is the shortening of the bond between the O atom of V41 and the N atom of L44. While in 6 M it is 0.2 Å shorter than in WT and does not cause any local structural difference, in 10 M the shortening is 0.3 Å and, together with the presence of the D43K mutation, results in a different organization of helix 2α N-terminus (41–46) and of loop 36–40 (Fig. S7). The 0.3 Å-shortened bond between residues F86 and I52 of the protein core does not seem to induce structural changes in either 6 M or 10 M. Besides, an automated calculation of tunnels in the three structures was performed using Caver PyMOL plugin v3.0. Although a similar number of tunnels was found in the three variants (13 in WT and 10 M, and 12 in 6 M), the average of the bottleneck radii, which gives the maximum probe size that can fit into the narrowest part of the tunnel, decreases from 0.751 Å in WT, to 0.725 Å in 6 M and 0.719 Å in 10 M. The narrowing of the tunnels in the three variants seems also to parallel their progressive stabilization. Finally, the impact of the stabilization on the flavodoxin molecular volume and internal cavities has also been assessed (Table S2). The WT protein exhibits the largest molecular volume (21,150 $Å^3$) and the highest number of internal cavities (5). The molecular volume of the stabilized mutants is slightly smaller and they contain less cavities of an overall smaller volume. However, their cavities are not equivalent in all cases, highlighting that stabilizing mutations can induce localized structural rearrangements without big changes in total volume.

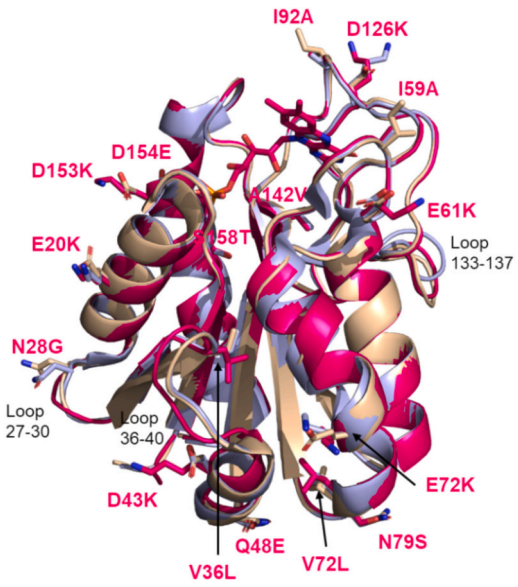

Fig. 6. Cartoon representation of the structural comparison of holoflavodoxin variants: 10 M (magenta; PDB ID: 9RXF), and 6 M (light blue; PDB ID: 5LJP) with WT (wheat; PDB ID: 1FLV). Key loop regions are highlighted, and residues mutated in the more stable 10 M variant are shown as stick representations, with mutations labeled in magenta.

Table 5
Kinetic parameters of WT, 6 M, 10 M, 3 M and 4 M flavodoxins.[a]

Mutant	K_M (μM)	k_{cat} (s^{-1})	k_{cat}/K_M (s^{-1} $μM^{-1}$)
WT[b]	33.0 ± 5.0	23.3 ± 1.6	0.70 ± 0.12
6 M	35.9 ± 0.6	21.2 ± 7.4	0.59 ± 0.21
10 M	43.6 ± 3.5	19.0 ± 8.0	0.44 ± 0.19
3 M	38.6 ± 9.1	6.3 ± 1.3	0.16 ± 0,05
4 M	101.1 ± 1.8	38.3 ± 6.3	0.38 ± 0.06

[a] The reported values of K_M and k_{cat} are means of two determinations ± SE
[b] Data taken from [45]

4. Discussion

Thermostabilization of 6 M apoflavodoxin [28,29], a highly stable apoflavodoxin variant obtained from the wild type protein over many years of as rational as possible trial an error based design, has been carried out exploiting the *Protposer* ranked list of potentially stabilizing mutations. As *Protposer* [20] is trained to identify mutations one by one and to compute their individual success probabilities, the more straightforward use of the *Protposer* list consists on producing individual mutants, testing stability and combining the stabilizing mutations. Alternatively, a potentially faster approach is to directly produce mutants encompassing several mutations. We have explored here the two strategies. On one hand, starting from 6 M, we created three multiple mutants (5 M1, 5 M2 and 5 M3) incorporating five new mutations in each one. Mutant 5 M1 recovered the three-state unfolding equilibrium of WT apoflavodoxin [44], experiencing a partial unfolding at a much lower temperature than 6 M, so it was not further considered. Of the two other mutants, 5 M2 had a ΔT_m of 4.4/4.0 °C (calculated from spectroscopic/DSC determinations) and 5 M3 of 2.6/2.6 °C. The subsequent combination of the 10 mutations in 5 M2 and 5 M3 into mutant 10 M,

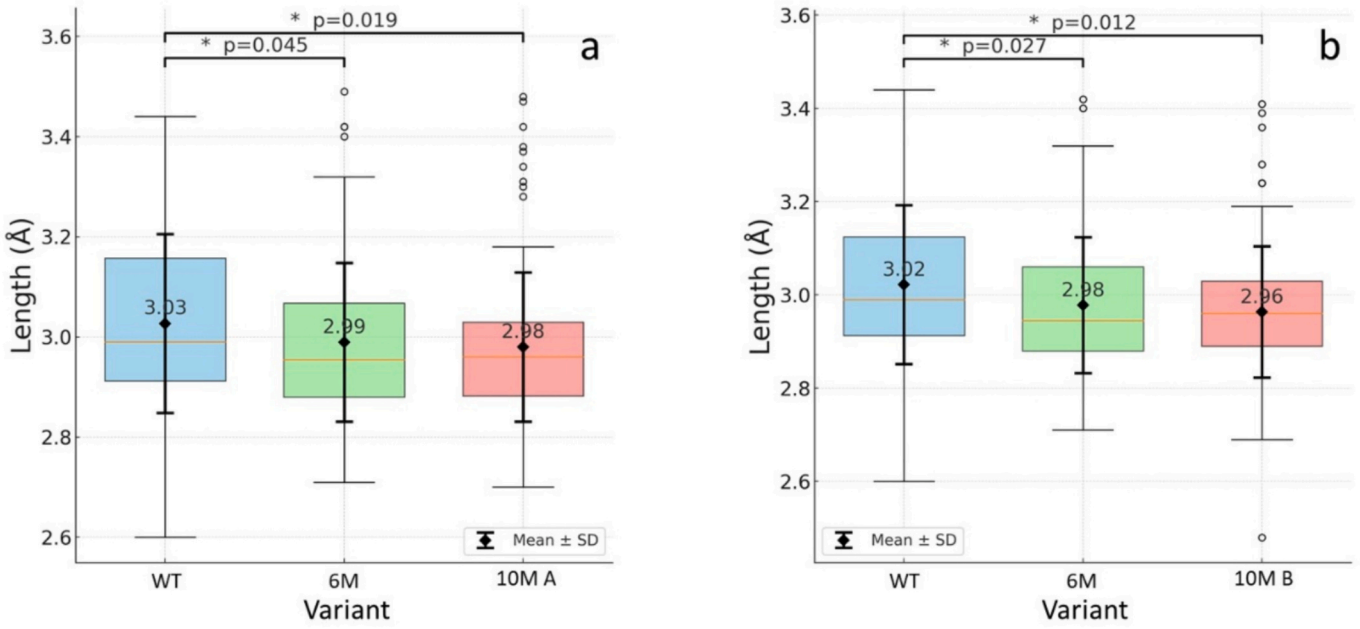

Fig. 7. Distribution of hydrogen bond lengths (Å) in (a) the wild-type (WT, $n = 114$) protein and its 6 M (n = 114) and 10 M A (n = 114) variants, or in (b) the wild-type (WT, $n = 110$) protein and its 6 M (n = 110) and 10 M B (n = 110) variants. Each box plot displays the interquartile range (IQR; 25th–75th percentiles) with the horizontal golden line inside representing the median. Whiskers extend to the most extreme data points within 1.5 × IQR from the quartiles. Black diamonds indicate the mean, with ticker black error bars and short caps showing the standard deviation (SD) of the mean. Given that the data did not meet the assumptions of normality and/or homogeneity of variances, group comparisons were performed using the non-parametric Mann–Whitney *U* test. Pairwise comparisons were performed between all groups. Significance levels are indicated only for statistically significant differences: $p < 0.05$ (*); non-significant comparisons are not shown. The analysis in (a) indicates that the 6 M variant differs significantly from WT ($p = 0.045$) and that the 10 M A variant differs significantly from WT (*$p = 0.019$), while no significant difference was detected between 6 M and 10 M A ($p = 0.796$). The analysis in (b) indicates that the 6 M variant differs significantly from WT ($p = 0.027$) and that the 10 M B variant differs significantly from WT (*$p = 0.012$), while no significant difference was detected between 6 M and 10 M B ($p = 0.808$).

produced a stabilizing effect which was slightly above additive (Fig. S8), raising the T_m by 9.2/8.6 °C. Given the strong stabilization achieved in 10 M and the low number of mutants tested to arrive to it, the approach followed of directly combining several mutations without individually testing them might have been considered the best choice. However, 10 M, albeit quite stable, showed a low tolerance to acidic pH, as well as a low tolerance to freezing and thawing. Thus, we sought to discard the mutations causing those issues and to identify those that increased the protein's stability. For that, we produced 10 single mutants. As many as 7/6 (from spectroscopic data/from DSC data) out of them displayed a T_m higher than 6 M. The three more stabilizing mutations (V36L, D153K and D154E) were then combined to produce 3 M and the forth mutation (N79S) was additionally included in 4 M. Both of these mutants were more stable than the 6 M reference variant (ΔT_ms of 6.1/6 °C for 3 M and 7.8/7.3 °C for 4 M), the stabilizing effects of the individual mutations combined being close to additive (Fig. S8). Unlike 10 M, neither of these mutants was negatively affected by acidic pH or freezing and thawing cycles, and they showed a higher reversibility in thermal unfolding than 10 M. Therefore, in terms of usability, the slightly lower stability of 4 M and 3 M relative to 10 M is more than compensated by their much better behavior in solution and their improved refoldability.

Increases in T_m usually pair with increases in conformational stability at lower temperatures [23], but this fact is not guaranteed by eq. 3 because changes in ΔH and ΔC_p also play a role in the extrapolation [50]. On the other hand, as *Protposer* has been trained with $\Delta\Delta G$ data, it produces a list of mutations that are expected to increase the stability by at least 0.5 kcal/mol, but whose effect on the T_m has not been calibrated. To test whether the thermostabilization achieved in 3 M and 4 M relative to 6 M, as well as that of 6 M relative to WT apoflavodoxin translate into conformational stabilization at 25.0 °C, we have used urea denaturation. Our data indicate that, at 25.0 °C, 6 M is about 2.7 kcal/mol more stable than the original WT and, more relevant for this work, they also indicate that 3 M and 4 M are approximately 2.5 kcal/mol more stable than 6 M, in line with the definition of success by *Protposer* ($\Delta\Delta G \geq 0.5$ kcal/mol) and with the expected success rates of the mutations combined in them. Finally, we have briefly analyzed potential consequences of the strong stabilization of apoflavodoxin in its three dimensional structure and electron transfer function. Comparison of WT [49], 6 M [29] and 10 M (this work) indicates that, as the protein becomes more stable, there is a mild trend toward compaction, reflected in a small reduction of cavity volume and a small shortening of hydrogen bond lengths. However, these small changes hardly modify the overall structure, and the same applies to the electron transfer efficiency of the protein which is similar in all the mutants tested.

5. Conclusions

Protposer is a straightforward and efficient computational tool for protein thermostabilization. Two cases can be considered to design a stabilizing strategy based on a *Protposer* mutation list. If the stability of the target protein is difficult to determine (e.g. the protein is difficult to express or purify in sufficient amount) a method that minimises the variants to be tested may be preferred. For that, several of the best ranked mutations may be simultaneously introduced in the WT and the more successful combination mutants may themselves be combined. However, for proteins that are easy to obtain and analyse, the proposed mutations are best tested one by one and the stabilizing ones combined, taking advantage of the fact that stabilizing effects tend to be additive. With this second approach, the unwanted effects from the odd, unexpectedly destabilizing mutations or from those that turn the protein unstable in certain solution conditions can be easily avoided. While the more artisanal stabilization of WT flavodoxin to produce the 6 M mutant took 15 years in our laboratory, the present stabilization of 6 M to obtain 4 M has been done in few months.

CRediT authorship contribution statement

Antonio Hidalgo-Toledo: Methodology, Investigation, Formal analysis, Data curation, Writing – original draft. **Darío Bazco:** Investigation. **Víctor Correa-Pérez:** Methodology, Data curation, Writing – original draft. **Marta Martínez-Júlvez:** Validation, Supervision, Resources, Methodology, Formal analysis, Data curation, Writing – original draft. **Javier Sancho:** Validation, Supervision, Resources, Project administration, Methodology, Funding acquisition, Formal analysis, Data curation, Conceptualization, Writing – review & editing, Writing – original draft.

Declaration of competing interest

All authors confirm that there are no known conflicts of interest associated with this publication and that there has been no significant financial support for this work that could have influenced its outcome.

Acknowledgments

We acknowledge financial support to JS from grants: 101004806 (European Union's Horizon 2020, MOSBRI); EFA080/01 (Interreg VI-A España-Francia-Andorra POCTEFA 2021-2027, OENOPROT); PID2022-141068NB-I00 (MICINN, Spain); and B23_24 and E45_23R (Gobierno de Aragon, Spain).

Appendix A. Supplementary data

Supplementary data to this article can be found online at https://doi.org/10.1016/j.ijbiomac.2025.148333.

Data availability

Data will be made available on request.

References

[1] K.A. Dill, J.L. MacCallum, The protein-folding problem, 50 years on, Science 338 (2012) (1979) 1042–1046, https://doi.org/10.1126/SCIENCE.1219021.
[2] M. Kesik-Brodacka, Progress in biopharmaceutical development, Biotechnol. Appl. Biochem. 65 (2018) 306–322, https://doi.org/10.1002/BAB.1617.
[3] P.J. Carter, A. Rajpal, Designing antibodies as therapeutics, Cell 185 (2022) 2789–2805, https://doi.org/10.1016/J.CELL.2022.05.029.
[4] J.M. Woodley, Protein engineering of enzymes for process applications, Curr. Opin. Chem. Biol. 17 (2013) 310–316, https://doi.org/10.1016/j.cbpa.2013.03.017.
[5] P. Chaisupa, R.C. Wright, State-of-the-art in engineering small molecule biosensors and their applications in metabolic engineering, SLAS Technol. 29 (2024) 100113, https://doi.org/10.1016/J.SLAST.2023.10.005.
[6] M. Blümel, J. Liu, I. de Jong, S. Weiser, J. Fast, J. Litowski, M. Shuman, S.B. Mehta, L. Amery, D.C.T. Tan, F. Jia, D. Shekhawat, C. Dagallier, M. Emamzadeh, A. Medina, C. Santos, F. Gasser, C. Urban, Current industry best practice on in-use stability and compatibility studies for biological products, J. Pharm. Sci. 112 (2023) 2332–2346, https://doi.org/10.1016/j.xphs.2023.05.002.
[7] H.P. Modarres, M.R. Mofrad, A. Sanati-Nezhad, Protein thermostability engineering, RSC Adv. 6 (2016) 115252–115270, https://doi.org/10.1039/C6RA16992A.
[8] K. Xu, H. Fu, Q. Chen, R. Sun, R. Li, X. Zhao, J. Zhou, X. Wang, Engineering thermostability of industrial enzymes for enhanced application performance, Int. J. Biol. Macromol. 291 (2025) 139067, https://doi.org/10.1016/J.IJBIOMAC.2024.139067.
[9] Y. Dehouck, J.M. Kwasigroch, D. Gilis, M. Rooman, PoPMuSiC 2.1: a web server for the estimation of protein stability changes upon mutation and sequence optimality, BMC Bioinf. 12 (2011) 1–12, https://doi.org/10.1186/1471-2105-12-151/METRICS.
[10] J. Schymkowitz, J. Borg, F. Stricher, R. Nys, F. Rousseau, L. Serrano, The FoldX web server: an online force field, Nucleic Acids Res. 33 (2005), https://doi.org/10.1093/NAR/GKI387.
[11] E. Capriotti, P. Fariselli, R. Casadio, I-Mutant2.0: predicting stability changes upon mutation from the protein sequence or structure, Nucleic Acids Res. 33 (2005), https://doi.org/10.1093/NAR/GKI375.
[12] M. Musil, J. Stourac, J. Bendl, J. Brezovsky, Z. Prokop, J. Zendulka, T. Martinek, D. Bednar, J. Damborsky, FireProt: web server for automated design of thermostable proteins, Nucleic Acids Res. 45 (2017) W393–W399, https://doi.org/10.1093/NAR/GKX285.
[13] J.J. Weinstein, A. Goldenzweig, S.Y. Hoch, S.J. Fleishman, PROSS 2: a new server for the design of stable and highly expressed protein variants, Bioinformatics 37 (2021) 123–125, https://doi.org/10.1093/BIOINFORMATICS/BTAA1071.
[14] R.F. Alford, A. Leaver-Fay, J.R. Jeliazkov, M.J. O'Meara, F.P. DiMaio, H. Park, M. V. Shapovalov, P.D. Renfrew, V.K. Mulligan, K. Kappel, J.W. Labonte, M.S. Pacella, R. Bonneau, P. Bradley, R.L. Dunbrack, R. Das, D. Baker, B. Kuhlman, T. Kortemme, J.J. Gray, The Rosetta all-atom energy function for macromolecular modeling and design, J. Chem. Theory Comput. 13 (2017) 3031–3048, https://doi.org/10.1021/ACS.JCTC.7B00125.
[15] F. Pucci, K.V. Bernaerts, J.M. Kwasigroch, M. Rooman, Quantification of biases in predictions of protein stability changes upon mutations, Bioinformatics 34 (2018) 3659–3665, https://doi.org/10.1093/BIOINFORMATICS/BTY348.
[16] O. Buß, J. Rudat, K. Ochsenreither, FoldX as protein engineering tool: better than random based approaches? Comput. Struct. Biotechnol. J. 16 (2018) 25–33, https://doi.org/10.1016/J.CSBJ.2018.01.002.
[17] D.R. Usmanova, N.S. Bogatyreva, J.A. Bernad, A.A. Eremina, A.A. Gorshkova, G. M. Kanevskiy, L.R. Lonishin, A.V. Meister, A.G. Yakupova, F.A. Kondrashov, D. N. Ivankov, Self-consistency test reveals systematic bias in programs for prediction change of stability upon mutation, Bioinformatics 34 (2018) 3653–3658, https://doi.org/10.1093/BIOINFORMATICS/BTY340.
[18] J. Fang, A critical review of five machine learning-based algorithms for predicting protein stability changes upon mutation, Brief. Bioinform. 21 (2020) 1285–1292, https://doi.org/10.1093/BIB/BBZ071.
[19] K.T. Bæk, K.P. Kepp, Data set and fitting dependencies when estimating protein mutant stability: toward simple, balanced, and interpretable models, J. Comput. Chem. 43 (2022) 504–518, https://doi.org/10.1002/JCC.26810.
[20] H. García-Cebollada, A. López, J. Sancho, Protposer: the web server that readily proposes protein stabilizing mutations with high PPV, Comput. Struct. Biotechnol. J. 20 (2022) 2415–2433, https://doi.org/10.1016/j.csbj.2022.05.008.
[21] C.G. Genzor, A. Perales-Alcon, J. Sancho, A. Romero, Closure of a tyrosine/tryptophan aromatic gate leads to a compact fold in apo flavodoxin, Nat. Struct. Biol. 3 (1996) 329–332, https://doi.org/10.1038/NSB0496-329.
[22] J. Estrada, P. Echenique, J. Sancho, Predicting stabilizing mutations in proteins using Poisson-Boltzmann based models: study of unfolded state ensemble models and development of a successful binary classifier based on residue interaction energies, Phys. Chem. Chem. Phys. 17 (2015) 31044–31054, https://doi.org/10.1039/C5CP04348D.
[23] L.A. Campos, M.M. Garcia-Mira, R. Godoy-Ruiz, J.M. Sanchez-Ruiz, J. Sancho, Do proteins always benefit from a stability increase? Relevant and residual stabilisation in a three-state protein by charge optimisation, J. Mol. Biol. 344 (2004) 223–237, https://doi.org/10.1016/j.jmb.2004.09.047.
[24] J. López-Llano, L.A. Campos, J. Sancho, J. Sancho, α-helix stabilization by alanine relative to glycine: roles of polar and apolar solvent exposures and of backbone entropy, Proteins Struct. Funct. Genet. 64 (2006) 769–778, https://doi.org/10.1002/prot.21041.
[25] M.P. Irún, S. Maldonado, J. Sancho, Stabilization of apoflavodoxin by replacing hydrogen-bonded charged asp or Glu residues by the neutral isosteric Asn or Gln, Protein Eng. 14 (2001) 173–181, https://doi.org/10.1093/PROTEIN/14.3.173.
[26] M. Bueno, N. Cremades, J.L. Neira, J. Sancho, Filling small, empty protein cavities: structural and energetic consequences, J. Mol. Biol. 358 (2006) 701–712, https://doi.org/10.1016/j.jmb.2006.02.060.
[27] S. Ayuso-Tejedor, O. Abián, J. Sancho, Underexposed polar residues and protein stabilization, Protein Eng. Des. Sel. 24 (2011) 171–177, https://doi.org/10.1093/PROTEIN/GZQ072.
[28] E. Lamazares, I. Clemente, M. Bueno, A. Velázquez-Campoy, J. Sancho, Rational stabilization of complex proteins: a divide and combine approach, Sci. Rep. 5 (2015), https://doi.org/10.1038/srep09129.
[29] E. Lamazares, S. Vega, P. Ferreira, M. Medina, J.J. Galano-Frutos, M. Martínez-Júlvez, A. Velázquez-Campoy, J. Sancho, Direct examination of the relevance for folding, binding and electron transfer of a conserved protein folding intermediate, Phys. Chem. Chem. Phys. 19 (2017) 19021–19031, https://doi.org/10.1039/c7cp02606d.
[30] C.G. Genzor, A. Beldarraín, C. Gómez-Moreno, J.L. López-Lacomba, M. Cortijo, J. Sancho, Conformational stability of apoflavodoxin, Protein Sci. 5 (1996) 1376, https://doi.org/10.1002/PRO.5560050716.
[31] D.E. Edmondson, G. Tollin, Chemical and physical characterization of the Shethna flavoprotein and apoprotein and kinetics and thermodynamics of flavin analog binding to the apoprotein, Biochemistry 10 (1971) 124–132, https://doi.org/10.1021/BI00777A019.
[32] J. Sancho, The stability of 2-state, 3-state and more-state proteins from simple spectroscopic techniques... plus the structure of the equilibrium intermediates at the same time, Arch. Biochem. Biophys. 531 (2013) 4–13, https://doi.org/10.1016/j.abb.2012.10.014.
[33] J. López-Llano, L.A. Campos, M. Bueno, J. Sancho, Equilibrium Φ-analysis of a molten globule: the 1-149 apoflavodoxin fragment, J. Mol. Biol. 356 (2006) 354–366, https://doi.org/10.1016/j.jmb.2005.10.086.
[34] C.N. Pace, B.A. Shirley, J.A. Thomson, Measuring the conformational stability of a protein, in: Protein Structure: A Practical Approach, 1989, pp. 311–330.
[35] W. Kabsch, Automatic indexing of rotation diffraction patterns, J. Appl. Crystallogr. 21 (1988) 67–72, https://doi.org/10.1107/S0021889887009737.
[36] P. Evans, Scaling and assessment of data quality, Acta Crystallogr. D Biol. Crystallogr. (2006) 72–82, https://doi.org/10.1107/S0907444905036693.
[37] J. Agirre, M. Atanasova, H. Bagdonas, C.B. Ballard, A. Baslé, J. Beilsten-Edmands, R.J. Borges, D.G. Brown, J.J. Burgos-Mármol, J.M. Berrisford, P.S. Bond, I. Caballero, L. Catapano, G. Chojnowski, A.G. Cook, K.D. Cowtan, T.I. Croll, J. Debreczeni, N.E. Devenish, E.J. Dodson, T.R. Drevon, P. Emsley, G. Evans, P.

R. Evans, M. Fando, J. Foadi, L. Fuentes-Montero, E.F. Garman, M. Gerstel, R. J. Gildea, K. Hatti, M.L. Hekkelman, P. Heuser, S.W. Hoh, M.A. Hough, H. T. Jenkins, E. Jiménez, R.P. Joosten, R.M. Keegan, N. Keep, E.B. Krissinel, P. Kolenko, O. Kovalevskiy, V.S. Lamzin, D.M. Lawson, A.A. Lebedev, A.G. W. Leslie, B. Lohkamp, F. Long, M. Malý, A.J. McCoy, S.J. McNicholas, A. Medina, C. Millán, J.W. Murray, G.N. Murshudov, R.A. Nicholls, M.E.M. Noble, R. Oeffner, N.S. Pannu, J.M. Parkhurst, N. Pearce, J. Pereira, A. Perrakis, H.R. Powell, R. J. Read, D.J. Rigden, W. Rochira, M. Sammito, F.S. Rodríguez, G.M. Sheldrick, K. L. Shelley, F. Simkovic, A.J. Simpkin, P. Skubak, E. Sobolev, R.A. Steiner, K. Stevenson, I. Tews, J.M.H. Thomas, A. Thorn, J.T. Valls, V. Uski, I. Usón, A. Vagin, S. Velankar, M. Vollmar, H. Walden, D. Waterman, K.S. Wilson, M. D. Winn, G. Winter, M. Wojdyr, K. Yamashita, The CCP4 suite: integrative software for macromolecular crystallography, Acta Crystallogr. D Struct. Biol. 79 (2023) 449–461, https://doi.org/10.1107/S2059798323003595.

[38] A. Vagin, A. Teplyakov, MOLREP: an automated program for molecular replacement, J. Appl. Crystallogr. 30 (1997) 1022–1025, https://doi.org/10.1107/S0021889897006766.

[39] G.N. Murshudov, A.A. Vagin, E.J. Dodson, Refinement of macromolecular structures by the maximum-likelihood method, Acta Crystallogr. D Biol. Crystallogr. 53 (1997) 240–255, https://doi.org/10.1107/S0907444996012255.

[40] P. Emsley, B. Lohkamp, W.G. Scott, K. Cowtan, Features and development of coot, Acta Crystallogr. D Biol. Crystallogr. 66 (2010) 486–501, https://doi.org/10.1107/S0907444910007493.

[41] L. Schrödinger, W. DeLano, PyMOL, 2020.

[42] P.J.A. Cock, T. Antao, J.T. Chang, B.A. Chapman, C.J. Cox, A. Dalke, I. Friedberg, T. Hamelryck, F. Kauff, B. Wilczynski, M.J.L. De Hoon, Biopython: freely available Python tools for computational molecular biology and bioinformatics, Bioinformatics 25 (2009) 1422–1423, https://doi.org/10.1093/bioinformatics/btp163.

[43] L.A. Campos, M. Bueno, J. Lopez-Llano, M.Á. Jiménez, J. Sancho, Structure of stable protein folding intermediates by equilibrium φ-analysis: the apoflavodoxin thermal intermediate, J. Mol. Biol. 344 (2004) 239–255, https://doi.org/10.1016/j.jmb.2004.08.081.

[44] M.P. Irún, M.M. Garcia-Mira, J.M. Sanchez-Ruiz, J. Sancho, Native hydrogen bonds in a molten globule: the apoflavodoxin thermal intermediate, J. Mol. Biol. 306 (2001) 877–888, https://doi.org/10.1006/jmbi.2001.4436.

[45] M. Medina, M. Martínez-Júlvez, J.K. Hurley, G. Tollin, C. Gómez-Moreno, Involvement of glutamic acid 301 in the catalytic mechanism of ferredoxin-NADP+ reductase from Anabaena PCC 7119, Biochemistry 37 (1998) 2715–2728, https://doi.org/10.1021/BI971795Y.

[46] G. Goñi, B. Herguedas, M. Hervás, J.R. Peregrina, M.A. De la Rosa, C. Gómez-Moreno, J.A. Navarro, J.A. Hermoso, M. Martínez-Júlvez, M. Medina, Flavodoxin: a compromise between efficiency and versatility in the electron transfer from photosystem I to ferredoxin-NADP(+) reductase, Biochim. Biophys. Acta 1787 (2009) 144–154, https://doi.org/10.1016/J.BBABIO.2008.12.006.

[47] M. Martínez-Júlvez, M. Medina, C. Gómez-Moreno, Ferredoxin-NADP c reductase uses the same site for the interaction with ferredoxin and flavodoxin, 1999.

[48] T. Mayoral, M. Martínez-Júlvez, I. Pérez-Dorado, J. Sanz-Aparicio, C. Gómez-Moreno, M. Medina, J.A. Hermoso, Structural analysis of interactions for complex formation between ferredoxin-NADP+ reductase and its protein partners, Proteins 59 (2005) 592–602, https://doi.org/10.1002/PROT.20450.

[49] S.T. Rao, F. Shaffie, C. Yu, K.A. Satyshur, B.J. Stockman, J.L. Markley, M. Sundaralingam, Structure of the oxidized long-chain flavodoxin from anabaena 7120 at 2 å resolution, Protein Sci. 1 (1992) 1413–1427, https://doi.org/10.1002/PRO.5560011103.

[50] W.J. Becktel, J.A. Schellman, Protein stability curves, Biopolymers 26 (1987) 1859–1877, https://doi.org/10.1002/BIP.360261104.